



Original Research Article

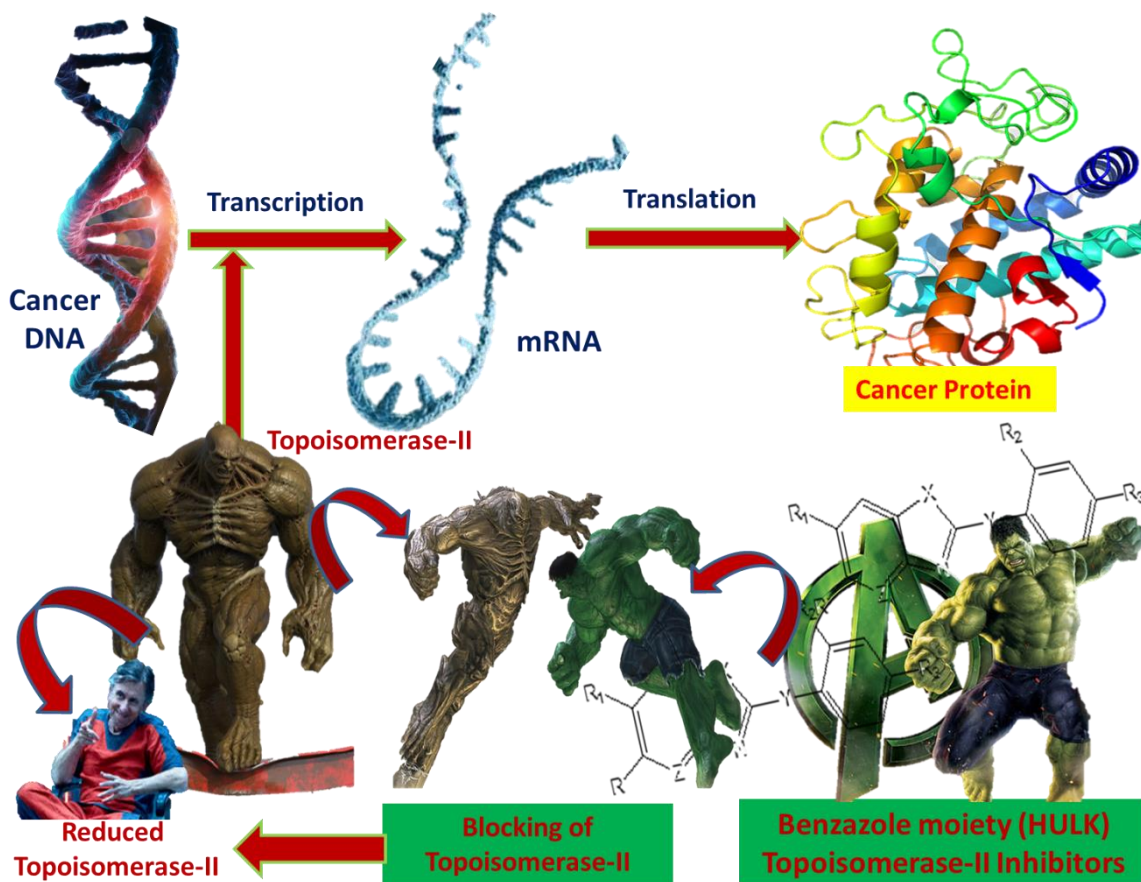
Evaluation of novel topoisomerase II inhibitors as anti-cancer agents through advanced computational strategies.

Mrs. Bhagyashree Warude¹, Mr. Amol B. Kumbhar², Dr. Jeevan Dhumal²,
Ms. Priyanka Chhajed¹, Amrita Verma Pargaien³, Dr. Manisha Savaliram Kedar⁴,
Dr. Swati N. Deshmukh⁵ and Dr. Aniket Garud^{*1}.

1. SJVPM's, Rasiklal M. Dhariwal Institute of Pharmaceutical Education & Research, Chinchwad, Pune, India. 411019.
2. RJSPM's College of Pharmacy, Duldulgaon, Moshi Alandi Road, Pune, Maharashtra, India.
3. College of Pharmacy Graphic Era Hill University Bhimtal.
4. Amrutvahini Institute of Pharmacy, Sangamner 422605.
5. CAYMET's, Siddhant College of Pharmacy, Sudumbare, Pune, India.

Corresponding author- draniketgarud@gmail.com

Abstract:



Over the past ten years, there have been a surprising number of advancements in the discovery of anticancer drugs. The development of selective topoisomerase II inhibitors has been a constant endeavour for more than 30 years. Eukaryotic cells require the enzyme DNA topoisomerase II to function. The DNA helix's topology is altered. The enzyme has a biological advantage, but it also has a pharmacological benefit because many anticancer drugs choose to target it. We have improved the benzazole moiety by employing molecular modelling studies in an effort to generate effective and harmless anti-neoplastic medicines. Results of 2D and 3D QSAR experiments for a series of 23 compounds are presented in this study. Results of 2D and 3D QSAR investigations for a series of 23 compounds including 5, 6-substituted-2-(2,4-disubstituted phenyl)-H-Benzazole derivatives are presented in this work. Using the partial least squares approach and principle component analysis, 2D QSAR experiments generated significantly effective prediction models with high cross-validated r^2 values of 0.7308 & 0.8443, respectively. Using the SA-KNN approach, 3D QSAR studies generated r^2 of 0.7647 and q^2 of 0.5551. Molecular modelling studies, such as 2D, 3D QSAR and docking studies, were carried out to gain detailed insights of the steric, electrostatic, and hydrophobic features required around the benzazole pharmacophore in order to better understand the relationship between structure and biological activity and to optimise the pharmacophore for design for New Chemical Entities (NCEs) with the better selectivity and subsequently better potency. In order to ensure the Drug like pharmacokinetic profile of the designed NCEs with the aid of Schrodinger Inc. software, docking and ADME properties of benzazole analogues were examined. Results were found to be comparable with standards and indicated that benzazole analogues have good binding affinity for topoisomerase II enzyme at ATP binding site using 1zxm pdb. Adenosine nucleotide triphosphate was reported to bind more selectively in the active binding pocket of 1ZXM enzyme and was compared to marketed medication Novobiocin in 4 out of 20 constructed NCEs.

In conclusion, the theoretical justification for pharmacophore optimization was confirmed, and it will now undergo wet lab work, specifically manufacturing and biological testing utilising the cell line assay. This paper will show the results of the current research activity and the in-depth research studies.

Key Words: Topoisomerase II inhibitor, Benzoxazole derivatives, LeadGrow, NCEs, 2D QSAR, 3D QSAR, Docking.

DOI Number: 10.48047/nq.2022.20.19.NQ99024

NeuroQuantology2022; 20(19):264-294

Introduction-

A nuclear enzyme called TOPOISOMERASE II (topo II) is essential for untying DNA tangles in the chromosomes during chromosome

segregation and replication, transcription, and cell division. It is a homodimer in its active state and a 170 kDa protein. Using a double-strand-passage mechanism, the



enzyme catalyses a number of ATP-dependent DNA topoisomerization events, including the relaxing of both positive and negative supercoiled DNA, catenation/decatenation, and knotting/unknotting. [1–6]

Topoisomerase II is the target of some of the most potent anticancer medications now being utilised to treat human cancers, in addition to its crucial physiological roles. [7-14] According to A.K. Larsen et al. (2003)[15], Antineoplastic drugs used to treat sarcomas, haematological malignancies, breast, lung, and prostate cancer commonly target the nuclear enzyme DNA topoisomerase II. All topoisomerase II-directed substances are capable of obstructing the catalytic cycle at least in part. With protomer molecular masses ranging from 160 to 180 kDa, topoisomerase II performs as a homodimeric enzyme [16,17]. Topoisomerase II and its cellular functions likely demonstrate both their physiological regulation and enzymological traits. Topoisomerase II levels are closely related to the proliferative state of the cell, even though their concentrations are rather consistent throughout cell and growth cycles. Therefore, the isoform is undoubtedly in charge of topoisomerase II's "housekeeping" duties, and the isoform is probably the type II enzyme that unlinks daughter chromosomes after replication [18]. Topoisomerase II-targeting medications fall into two categories. The majority of clinically useful drugs in the first class, such as etoposide, doxorubicin, and

mitoxantrone, enhance the concentrations of Topo2:DNA covalent complexes. These substances are known as Topoisomerase II poisons because they create a "lesion" that contains DNA strand breaks and proteins covalently attached to DNA. The catalytic activity of Topoisomerase II is inhibited by a second class of substances, but their levels of Topoisomerase II covalent complexes are not increased. The crucial enzymatic activity of Topoisomerase II is assumed to be the mechanism by which this second class of drugs, known as catalytic inhibitors[19], kills cells.

Therefore, any mechanism that results in altered Topoisomerase II binding to medicines or DNA and decreased creation of cleavable complexes can result in resistance against traditional Topoisomerase II -inhibiting medications. In fact, it has been shown that decreased Topoisomerase II catalytic activity can influence cancer cells' treatment resistance [21]. [20] This phenotype was known as altered Topo II multidrug resistance because these drug-resistant tumour cells revealed cross resistance to other medications. Both reduced expression levels of the two Topo II isoforms as well as missense mutations in the genes encoding the Topo II isoenzyme can contribute to the decline in Topo II activity. [22] Designing alternative therapeutic techniques that can be applied for the treatment of drug-resistant cancer cells is crucial since drug resistance is a significant barrier to the successful treatment of neoplastic illnesses. The creation of alternative Topoisomerase II



targeting medications without cross resistance in cancer cells displaying a drug-resistant phenotype against traditional Topo II inhibitors is one of these strategies.

So, after testing a number of derivatives of benzoxazoles, benzimidazoles, and related fused heterocyclic compounds for their inhibitory effects on eukaryotic Topoisomerase II in a cell-free environment, In this study, they discovered the potential antineoplastic activity of these substances in various human cancer cell lines derived from various tumour entities and found that some of these compounds had Topoisomerase II inhibiting activity under cell-free conditions. They also developed multidrug-resistant sub lines with decreased Topoisomerase II expression. Traditional names for substances that can stabilise the covalent DNA topoisomerase II complex, also referred to as the cleavable complex, include etoposide, which is also known as a topoisomerase II poison. Substances that affect any of the other steps in the catalytic cycle are known as catalytic inhibitors, such as novobiocine bisdioxypiperazine derivatives. [23,24]

In the current study, we report that recombinant topoisomerase II's N-terminal ATPase activity is inhibited by benzazole derivatives. To do molecular docking studies, we chose the pdb 1ZXM, which has a co-crystallized ligand. Less effective inhibition of the enzyme's ATPase function

by benzazole analogues is revealed by mutation of key amino acids close to the ligand-binding region. When seen as a whole, these findings offer guidance for the design of newer medicinal medicines with distinct selectivity.

Computational studies-

One of the effective approaches for creating highly active compounds is computational modelling. As screening techniques for the development of New Chemical Entities (NCEs), numerous QSAR studies were created and published. As seen in Figure 1, 2D QSAR and 3D QSAR studies using Multiple Linear Regression (MLR) Analysis and k Nearest Neighbor Molecular Field Analysis (kNN MFA), respectively, were conducted to further explore the structural requirements of selected series of Benzazole derivatives for their antiproliferative activity. NCEs were created utilising the QSAR model's findings.

2. Results and Discussion: -

2.1 QSAR study

For the purpose of comparing the chemical composition (structure) of compounds with their antiproliferative activity, a total of 23 compounds were employed, for which absolute IC₅₀ values were given [25].



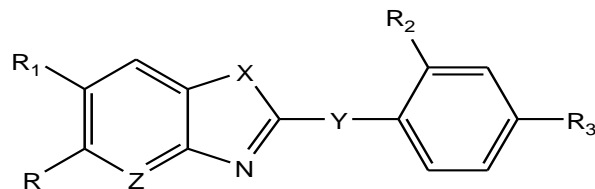


Fig: 1 General strcture of benzazole showing sites of substitution pattern.

Table 1 The selected series of benzazole derivatives as eukaryotic topoisomerase II inhibitors as anticancer activity with IC₅₀ & PIC₅₀.

Molecule No	X	Y	Z	R	R ₁	R ₂	R ₃	IC ₅₀	PIC ₅₀
1	-O-	---	-CH=	-H-	-NO ₂	-H-	-OCH ₃	17.0	-1.23
2	-O-	---	-CH=	-NH ₂	-H-	-C ₂ H ₅	-H-	115.5	-2.062
3	-O-	----	-CH=	-CH ₃	-H-	-H-	-CH ₃	44.4	-1.647
4	-O-	----	-CH=	-NO ₂	-H-	-H-	-H-	32.4	-1.5105
5	-O-	----	-CH=	-CH ₃	-H-	-H-	-H-	128.4	-2.1085
6	-O-	----	-CH=	-NO ₂	-H-	-H-	-H-	22.4	-1.3502
7	-O-	----	-N=	-H	-H-	-H-	-H-	45.6	-1.6589
8	-O-	----	-N=	-H	-H	-H	-H-	119.5	-2.0773
9	-O-	----	-N=	-H	-H-	-H-	-H-	91.2	-1.9599
10	-O-	-CH ₂	-CH=	-H	-H-	-H-	-H-	86.6	-1.9375
11	-NH-	-CH ₂	-CH=	-CH ₃	-H-	-H-	-H-	46.8	-1.6702
12	-NH-	-CH ₂	-CH=	-CH ₃	-H-	-H-	-H-	27.4	-1.4377
13	-NH-	-CH ₂ S	-CH=	-COOCH ₃	-H-	-H-	-H-	17.0	-1.2304
14	-NH-	CH ₂ O	-CH=	-NO ₂	-H-	-H-	-H-	28.4	-1.4533
15	-O-	---	-CH=	-Cl	-NO ₂	-NO ₂	-H-	101.9	-2.0081
16	-NH-	-C ₂ H ₄	-CH=	-H-	-H-	-H-	-H-	216.6	-2.3358
17	-O-	---	-CH=	-H-	-CH ₃	-H-	-F	433.2	-2.6366
18	-O-	---	-CH=	-H-	-CH ₃	-H-	-NO ₂	18.8	-1.2741
19	-O-	---	-CH=	-CH ₃	-H-	-H-	-OCH ₃	433.0	-2.6364
20	-O-	---	-N=	-H-	-H-	-C(CH ₃) ₃	-H-	108.3	-2.0346



21	-O-	CH ₂	-CH=	-CH ₃	-H-	-CH ₃	-H-	101.9	-2.0081
22	-S	CH ₂ O	-CH=	-H-	-H-	-H-	-H-	11..4	-1.0569
23	-NH	CH ₂	-CH=	-Cl	-H-	-H-	-H-	308.1	-2.4866

2.1.1 2D-QSAR studies:

Invariable columns were eliminated, and several descriptors were generated. Based on the biological and chemical diversity, the training and test sets were separated into 19 and 4 compounds, respectively. Utilizing simulated annealing (SA) as a variable selection technique, 2D-QSAR was carried out using partial least squares (PLS), principle component regression (PCR), and multiple linear regression (MLR). Using SA-PLS, SA-PCR, and SA-MLR combinations, various 2D QSAR models were created. In comparison to SA-PLS and SA-MLR, the SA-PCR produces the best predictive model. The calculated r² was 0.7308, the calculated r²CV was 0.6391, and the projected r² was 0.6291. Eq. 1 and the following provide the model equation. Table 2 shows statistical findings from the 2D QSAR investigation. Plot comparing actual biological activity versus anticipated activity following equation shown calculated predicted activity.

269

$$pKi=0.1652T_N_O_1+0.2439T_2_N_O+0.6078SulfursCount+ 0.0536T_2_2_7-2.6850. \text{ Eq.1}$$

Table 2 Results of 2D QSAR

Statistical Parameter	Regression Method		
	SA-PCR	SA-PLS	SA-MLR
r ²	0.8072	0.7443	0.7308
q ²	0.6391	0.5338	0.6348
F test	13.5749	14.5537	15.7045
pred_r ²	0.6291	0.6182	0.6638
pred_r ² se	0.1523	0.1748	0.3494
Positively Contributing Descriptors	T_N_O_1(38%) T_2_N_O(25.21%) SulfursCount(21.1%) T_2_2_7(18.1%)	T_2_O_4(30.88%) MMFF_15(37.01%) T_2_N_2(18.95%)	T_2_2_0(38%) T_C_S_5(31%) T_N_O_1(28%)
Negatively Contributing Descriptors	-----	FluorinesCount(13.16%)	T_O_F_4(24%)

Several QSAR models were created, but the best model, derived by the SA-PCR approach (Eq 1), was then utilised to predict activity based on the model's most promising statistical findings and



predictability. Tables 3 and 4, respectively, exhibit the observed and projected activity as well as the residual values of the training set and test set.

Table 3 Observed and predicted activity of the training set

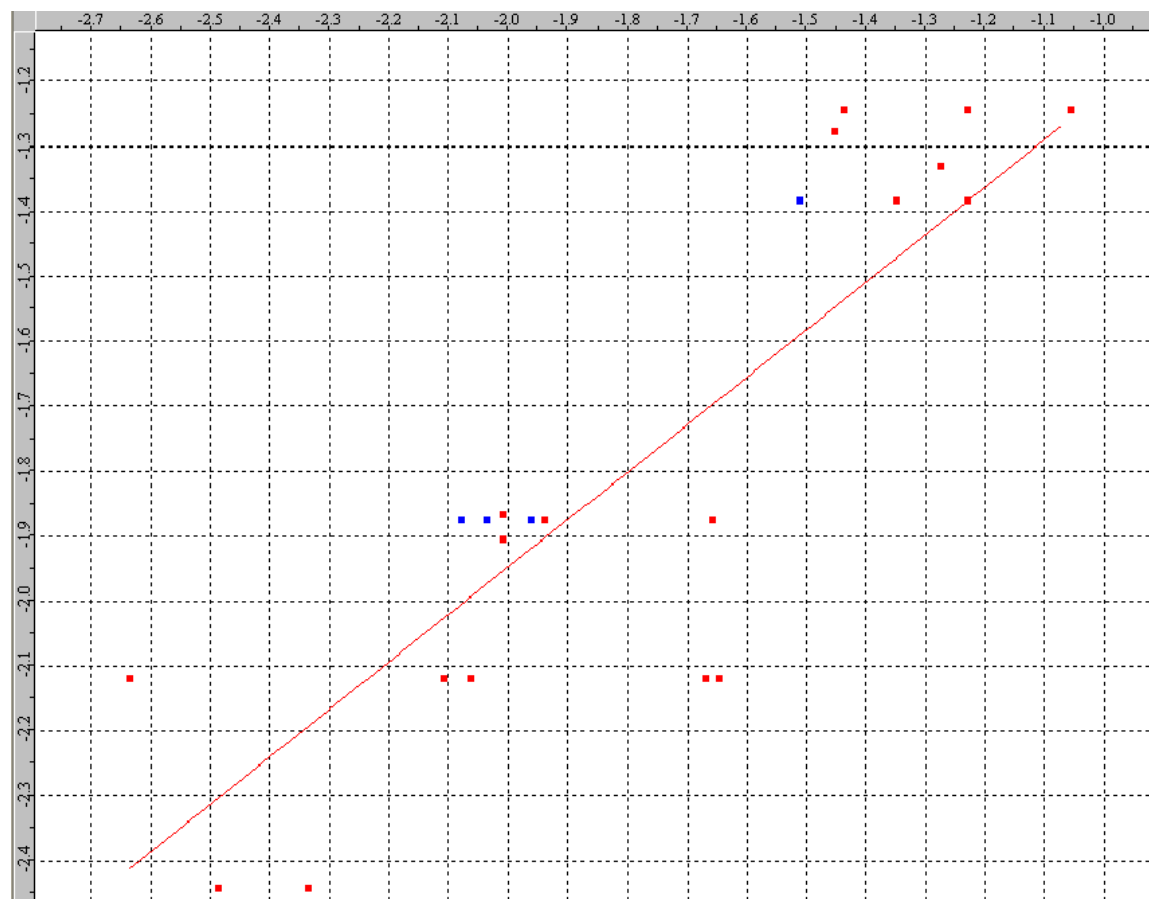
Molecule No.	Observed activity(IC ₅₀)	PIC ₅₀	Predicted Activity	Residual
23	308.1	-2.4866	-2.44115	-0.04545
1	17.0	-1.23	-1.38427	0.15427
2	115.5	-2.062	-2.11941	0.05741
3	44.4	-1.647	-2.11941	0.47241
5	128.4	-2.1085	-2.11941	0.01091
6	22.4	-1.3502	-1.38427	0.03407
7	45.6	-1.6589	-1.87552	0.21662
10	119.5	-1.9375	-1.87552	-0.06198
11	91.2	-1.6702	-2.11941	0.44921
12	86.6	-1.4377	-1.24349	-0.19421
13	46.8	-1.2304	-1.24349	0.01309
14	27.4	-1.4533	-1.27702	-0.17628
15	17.0	-1.4533	-1.27702	-0.17628
16	28.4	-2.0081	-1.86687	-0.14123
17	101.9	-2.3358	-2.44115	0.10535
18	216.6	-2.6366	-2.11941	-0.51719
19	433.2	-2.6364	-2.11941	-0.51699
21	101.9	-2.0081	-1.90493	-0.10317
22	11..4	-1.0569	-1.24349	0.18659

270

Table 4 Observed and predicted activity of test

Molecule No.	Observed activity(IC ₅₀)	PIC ₅₀	Predicted Activity	Residual
4	32.4	-1.5105	-1.38427	-0.12623
8	119.5	-2.0773	-1.87552	-0.20178
9	91.2	-1.9599	-1.87552	-0.08438
20	108.3	-2.0346	-1.87552	-0.15908





Red points = training set, Blue point = test set.

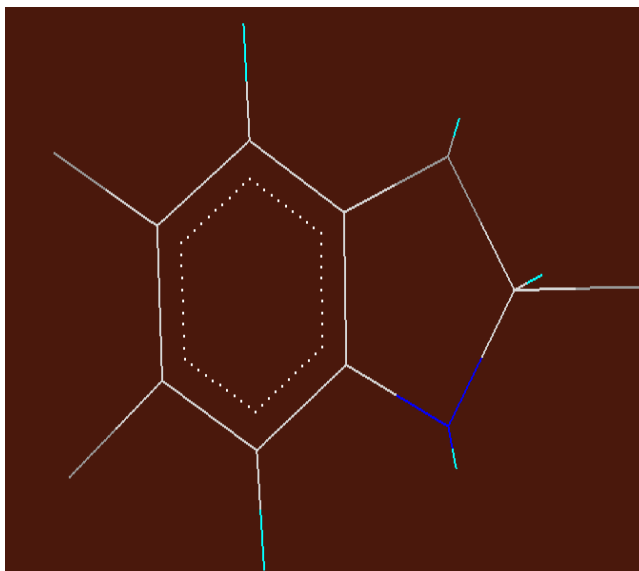
Fig. 2 Observed versus predicted activities of training and test set according to the model shown in equation-1

2.1.2 3D-QSAR studies-

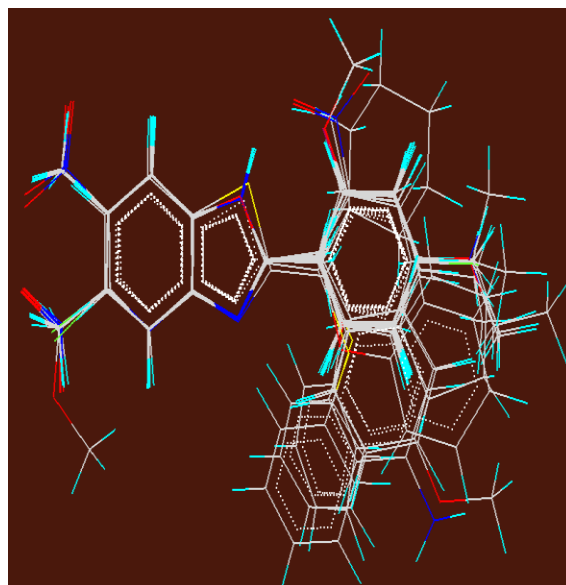
Using the template-based alignment technique, all of the optimised compounds were aligned.[26] Fig. 3a displays the template used for the alignment. Calculations were made for topological, steric, and electrostatic descriptors. The kNN- MFA, which applies the k-Nearest Neighbor principle, was used to carry out the 3D-QSAR experiments. The molecular field and biological activity are related by kNN-MFA. Utilizing SA-kNN, 3D QSAR models were created. An unknown member is categorised using this method based on the vast majority of its k-Nearest Neighbors in the training set. An adequate distance matrix is used to measure proximity (e.g. a molecular similarity measure calculated using field interactions of molecular structures) The SA-kNN-MFA method uses the SA variable selection process along with the kNN classification principle to create a 3D model. Prior to alignment, molecules were optimised using the MMFF energy minimization approach since optimization is a step that is required for accurate alignment of molecules around templates. and the



template-based alignment approach was used to perform the alignment of the given set of molecules, which is necessary for the kNN-MFA method (**Fig. 3b**).



(3.a)Top view of superimposed molecules as common template



(3.b)benzazoleDerivative using template base alignment method

The activity of the training set of 19 compounds was predicted using the set of aligned molecules that resulted. The data produced by the training set of compounds was used to forecast the behaviours of the test set of compounds. Table No. 5 lists the statistical outcomes that 3D QSAR models produced.

Table 5: -Comparison of the various statistical results of 3D QSAR generated by SA kNN-MFA Methods for benzazole derivatives.

Sr no	Parameters	SA kNN-MFA		
		Model A	Model B	Model C
1	q^2	0.5462	0.5007	0.5551
2	$Pred.r^2$	0.7594	0.6970	0.7647
3	$Q^2 SE$	0.3138	0.3291	0.3107
4	$Pred.r^2 SE$	0.2616	0.2935	0.2015
5	N	20	20	20
6	K Nearest Neighbor	3	2	4
Contributing descriptor				
7	Contributing steric parameter	-----	S_100(-0.0423, -0.0225) S_485(-0.0362,-0.0135) S_419(-0.0986,-0.0388)	S_215(-0.0094,-0.0092) S_419(-0.0484,-0.0475)
8	Contributing hydrophobic parameter	H_398(-0.0401, -0.0288)	-----	H_794(0.2590,0.3187)
9	Contributing electronic parameter	E_72(-0.0369,0.0721) E_811 (0.4397,0.8568)	E_81 (0.4397,0.8568)	E_291(-0.5790 ,-0.4344)

273

Model C has the highest levels of internal and external predictability ($q^2 = 0.5551$, $pre r^2 = 0.7647$). Additionally, compared to models A & B, the standard error (SE) of internal and external validation was extremely low, or $Pred r^2 se = 0.2015$. the final equation, which is given in eq. 2. The range of 3D data points produced within a rectangular grid Using SA kNN-MFA and the best model C, predictions for the contributions of steric and electrostatic data points are shown in parentheses in Fig 4.

In order to maximise the electronic and steric requirements around the pharmacophore, model C was adopted. Indicating that increasing the maximum number of Nearest Neighbors will boost the internal as well as external predictivity of 3D QSAR model, it also led to minimise the



error in predictability, the values of k Nearest Neighbor in all three models A, B, and C were determined to be 3, 2 and 4.

Plots of the observed vs anticipated activities using the model described in Eq. 2 and the contribution plot of the best model's electronic interaction are shown in Fig. 5 correspondingly. Table 6 displays the outcome of the training and test set's residual of the observed and anticipated activities.

$$pKi = 0.2590 H_{794} - 0.5790 E_{291} - 0.0094 S_{215} - 0.0484 \text{ (Eq. 2)}$$

Table 6 Observed and predicted activities of the training and test set.

Molecule no	IC ₅₀	PIC ₅₀	SA kNN MFA model	
			Predicted activity	Residual activity
1	17	-1.23	-1.2741	0.7781
2	115.5	-2.062	-2.0081	-0.0539
3	44.4	-1.647	-2.0081	-0.5901
4	32.4	-1.5105	-1.0569	0.4976
5	128.4	-2.1085	-2.0081	-0.6708
6	22.4	-1.3502	-1.4377	0.6844
7	45.6	-1.6589	-2.0346	0.8277
8	119.5	-2.0773	-2.4866	-0.4184
9*	91.2	-1.9599	-1.6589	-0.2897
10	86.6	-1.9375	-1.6702	-0.2673
11	46.8	-1.6702	-1.9375	0.2673
12	27.4	-1.4377	-1.3502	-0.875
13*	17	-1.2304	-1.4377	0.2073
14*	28.4	-1.4533	-1.4337	-0.0156
15	101.9	-2.0081	-2.062	0.0539
16	216.6	-2.3358	-2.4866	0.1508
17	433.2	-2.6366	-2.062	-0.5746
18	18.8	-2.2741	-1.23	-1.0441
19	433	-2.6364	-2.1085	-0.5279
20	108.3	-2.0346	-1.5689	-0.4657
21	101.9	-2.0081	-2.1085	0.1004
22	11.4	-2.0569	-1.5105	0.9415
23	308.1	-2.4866	-2.3358	-0.1508



***test set**

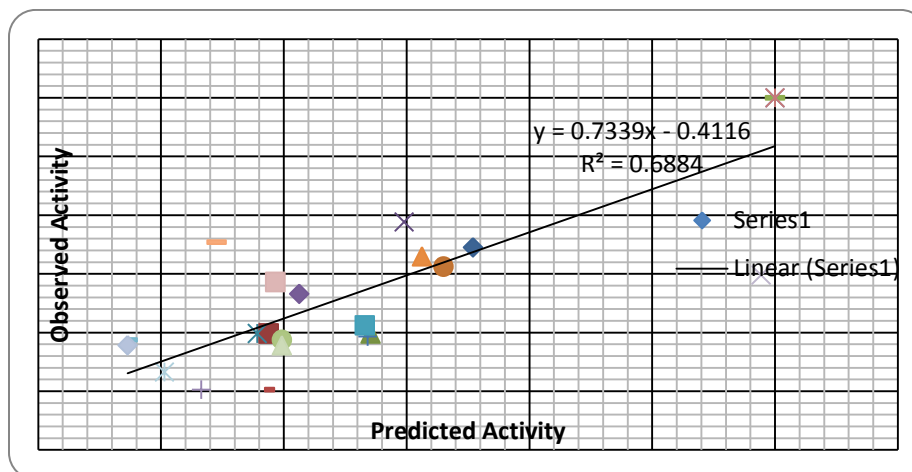


Fig. 5 Observed versus predicted activities according to the model shown in Eq.2

2.1.3 Interpretation of QSAR Studies: -

The BENZAZOL nucleus was optimised for selective inhibition of the Topoisomerase II inhibitors using the data from 2D and 3D QSAR tests. The magnitude and sign of each descriptor's regression coefficient make it easy to understand the contribution of each to a 2D QSAR PLS equation. When compared to other descriptors, a descriptor's coefficient magnitude demonstrates how much it contributes, and its sign reveals whether it is directly (+) or inversely (-) proportionate to the activity. The generated PLS Equation 1 showed that the descriptor MMFF 15, which is an atom type count descriptor based on MMFF atom types, performed the most significant important function (contribution around 37% for biological activity) in determining Topoisomerase II inhibitory action. This is an atom type count descriptor based on MMFF atom types and their count in each molecule, and the number "15" indicates how many times that atom type has been

identified in a particular molecule. This unmistakably shows that the urea molecule is necessary for increased biological activity in the molecule's pharmacophore. The next significant descriptor was T 2 O 4 (contribution to biological activity: about 30%). This alignment-independent descriptor defines the number of oxygen atoms in molecules that are isolated from other atoms (single or double bound) by 4 bond lengths. T 2 N 2, which contributes about 18.95% of the biological activity and is directly correlated with that activity, was the next significant descriptor. which is directly correlated with the activity and an alignment independent descriptor that counts the number of double bonds that are separated from the nitrogen atom by any other atom by a distance of two bonds. Fluorine count, which contributes about 13.10% to biological activity and is inversely proportional to it, is the final descriptor governing variation in activity. This suggests that the presence of fluorine substituents in



any position of the benzazole pharmacophore may be unfavourable or detrimental to the activity.

The hydrophobic electrostatic and steric requirements around the benzazole pharmacophore were optimised using 3D QSAR. Fig. 4 displays the 3D data points that were produced and added to the SA kNN MFA 3D QSAR model. Designing effective NCEs was aided by the range of property values for the generated data points. The range was calculated using the nearest neighbour set and the most active molecule to determine how the field values varied at the selected points. The points produced by the SA KNN MFA 3D QSAR model are specifically mentioned in table number 5 and correspond to the lattice points 215, 419, 794, and 291 for the steric, electrostatic, and hydrophobic interaction fields, respectively. These points made reference to the importance and necessity of the hydrophobic, electrostatic, and steric properties, as specified in the ranges in parenthesis, for the link between structure and activity and for the highest possible

biological activity of derivatives. The more hydrophobic group relevant for biological action is indicated by positive hydrophobic field descriptor. Negative electrostatic field descriptor values suggested that benzazole derivatives needed negative electrostatic potential to increase their biological activity. Therefore, around the benzazole pharmacophore, electronegative substituents were favoured at the site of generated data points E 291(-0.5790,-0.4344).

276

Similar to this, the negative steric descriptor values indicated that sterically less groups were necessary to surround the benzazole pharmacophore for maximum activity. Thus, the KNN-MFA models identify distinct local interacting chemical properties that are accountable for activity variation and thereby give convenient guidance for the design of novel compounds. Following a thorough review of the literature and the findings of molecular modelling studies carried out at our institute, the pharmacophore has been updated

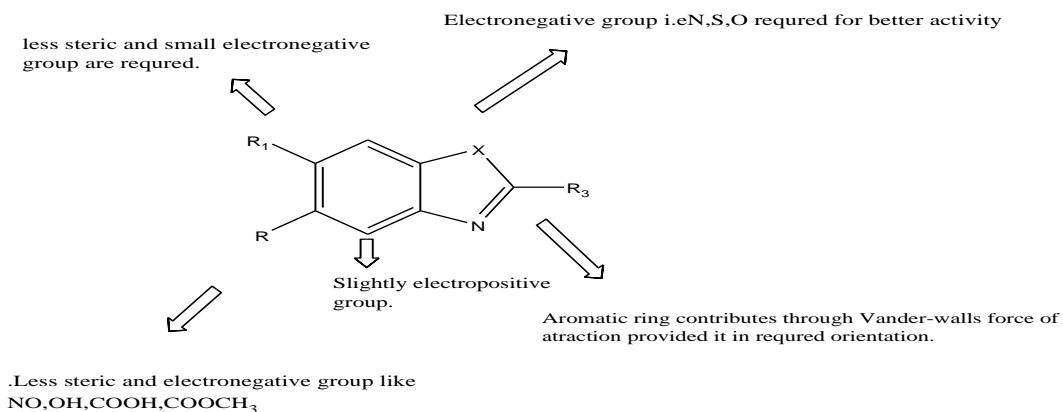


Fig 6 Optimise pharmacophore



2.2 NCE Design and Screening:

The electrostatic and steric requirements around the benzazole nucleus were optimised using the data from 2D and 3D QSAR investigations in order to increase the anticancer activity (Fig. 5). Because of the relevance of the benzimidazole group for anticancer activity at E 291(-0.5790,-0.4344), descriptors produced by the 2D QSAR equation indicated this. In the 3D QSAR depicted in, similar hydrophobic electrostatic and steric points produced around a common template or pharmacophore (Fig. 4).

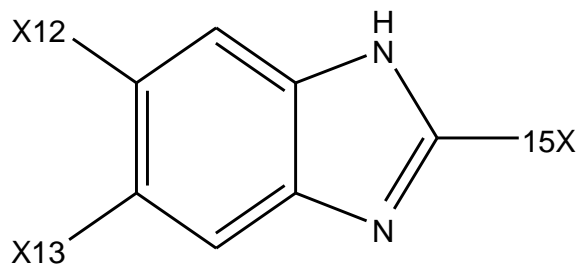
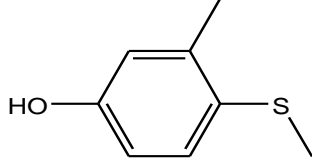
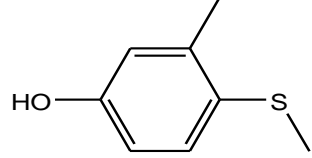
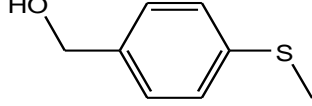
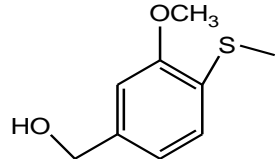
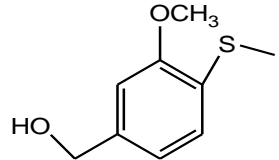

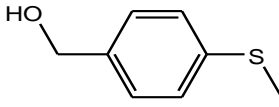
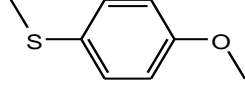
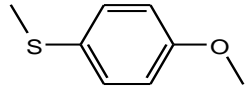
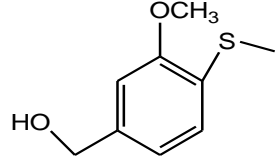
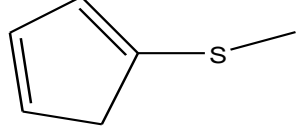


Fig.6 Template for CombiLib

Utilizing the Lipinski's rule-following CombiLib programme, more over three hundred compounds were produced; however, we only chose the 15 most active molecules based on their anticipated activity as determined by the PCR equation result presented in Table 7.

Table7 :- NCEs generated by CombiLib tool of V-Life Molecular Design Suite software

Sr no	Molecule no	12X	13X	15X	Predicted activity	Lipinski Screen	Lipinski Score
1	028	-NO ₂	-COOH		-0.92349	ADRXWS	6
2	025	-NO ₂	-COOH		-0.6749	ADRXWS	6
3	080	-COOH	-NO ₂		-0.66921	ADRXWS	6
4	056	-OH	-NO ₂		-0.80213	ADRXWS	6

5	055	-OH	-NO ₂		-0.53 178	ADRXWS	6
6	079	- COOH	-NO ₂		-0.7456	ADRXWS	6
7	026	-NO ₂	-COOH		-0.53999	ADRXWS	6
8	082	- COOH	-NO ₂		-0.62189	ADRXWS	6
9	058	-OH	-NO ₂		-0.6652	ADRXWS	6
10	<u>047</u>	-NO ₂	- CH ₂ OCOOCH 3		<u>-1.5853</u>	ADRXWS	6
11	<u>002</u>	-OME	-COOH		<u>-1.24349</u>	ADRXWS	6
12	083	- COOH	-NO ₂		-0.6772	ADRXWS	6
13	029	- COOH	-NO ₂		-0.5231	ADRXWS	6
14	<u>004</u>	-OME	-COOH		<u>-1.2349</u>	ADRXWS	6
15	060	-OH	-NO ₂		-0.83008	ADRXWS	6

Compounds qualifying are shown in Table 7 with ADRXWS strings for all required Lipinski's Screen/filter parameters. All six of Lipinski's screen parameters are satisfied by the relevant compound, according to the columns carrying the Lipinski's screen score and strings of alphabets in ADRXWS, and the screen score ranged from 1 to 6 depending on how many requirements were satisfied. The results show that Lipinski's screen's parameters are all being satisfied by designed NCEs. (See Table Number 7) Only 3 of the 15 design NCEs, namely 047,002,004, are compounds. When compared to the most potent compound from the original series used for 2D and 3D QSAR investigations, compound no. 22 (PIC50 -1.0569), it was discovered that predicted concentrations of 1.5853, 1.24349, and 1.2349 were less potent. According to the projected activity of the proposed molecule, the addition of sterically bulky groups like 3-methyl-4-(methylthio)phenol and (4-(methylthio)phenyl) methanol and an electron-withdrawing group at position 12X both greatly increased the activity of the compounds.

Molecular docking

The molecular docking programme Glide (5.0) was used to conduct the

investigations. Table 8 displays the molecular docking studies' hydrogen binding interactions and G score. Additionally, Table 9 provides a full examination of the interactions. Fig. 7 shows interactions between molecules nos. 28, 25, 80, and 55 and the protein's amino acid residues. This has greatly increased our confidence in the justification for the pharmacophore optimization. This demonstrates that we were successful in optimising the pharmacophore thanks to our thorough literature review, molecular modelling findings (2D & 3D QSAR) investigations, and SBDD outcomes more so than our scientific intuition.

The Topo2 enzyme (PDB Code 1ZXM) was docked with all of the developed compounds that shown good anticipated activity and adhered to Lipinski's rule to analyse the binding mode of the compounds. The results of these investigations were useful for further screening of created compounds to identify those with high binding affinities. Adenosine nucleotide triphosphate (ANP), which is contained in the 1ZXM pdb and is a typical Topo2 Atpase inhibitor, and other compounds were used to compare the binding modalities of the developed compounds.

279



Table 8 Results of molecular docking studies.

Sr. No.	Molecule No.	G-score	E-model	No.Of Hydrogn bond	No. of Good Vander waal interaction	No. of Bad Vander waal interaction	No. of Ugly Vander waal interaction
1	28	-10.02	-110.7	7	386	16	2
2	25	-9.93	-103.2	7	283	12	1
3	80	-9.90	-103.6	7	258	12	1
4	56	-9.87	-114.4	4	233	6	3
5	55	-9.83	-102.2	6	238	17	2
Standard	ANP	-9.82	-104.6	12	293	18	7
7	79	-9.77	-103.4	7	271	17	0
8	26	-9.70	-102.9	7	256	10	2
9	82	-9.67	-102.7	7	264	11	3
10	47	-.9.34	-107.5	3	231	8	3
11	02	-9.19	-93.3	4	293	14	3
12	83	-9.08	-103.5	6	263	9	2
13	29	-8.98	-104.2	6	264	14	0
14	04	-8.94	-87.7	5	370	17	6
Standard	Novobiosin e	-8.55	-60.9	3	441	20	1

##G-score –Key finding of overall SBDD studies.

The optimum docking poses for the co-crystallized inhibitor and its bound conformation were compared in order to assess the trustworthiness of the docking data. This was accomplished by withdrawing the co-crystallized ligand from their active site and re-docking it into the binding pocket in the crystal structure's conformation. With a root mean square deviation (RMSD) of 0.7, the docking method appeared to be trustworthy in predicting the binding mode of our drugs. The success of screening methods in structure-based drug design depends on the precise prediction of protein-ligand interaction geometries. Based on the Glide Score (G Score), Hydrogen Bonds (H-Bond), and Vander Waals (VDW) Interaction between the ligands and receptor, the docking data were assessed.



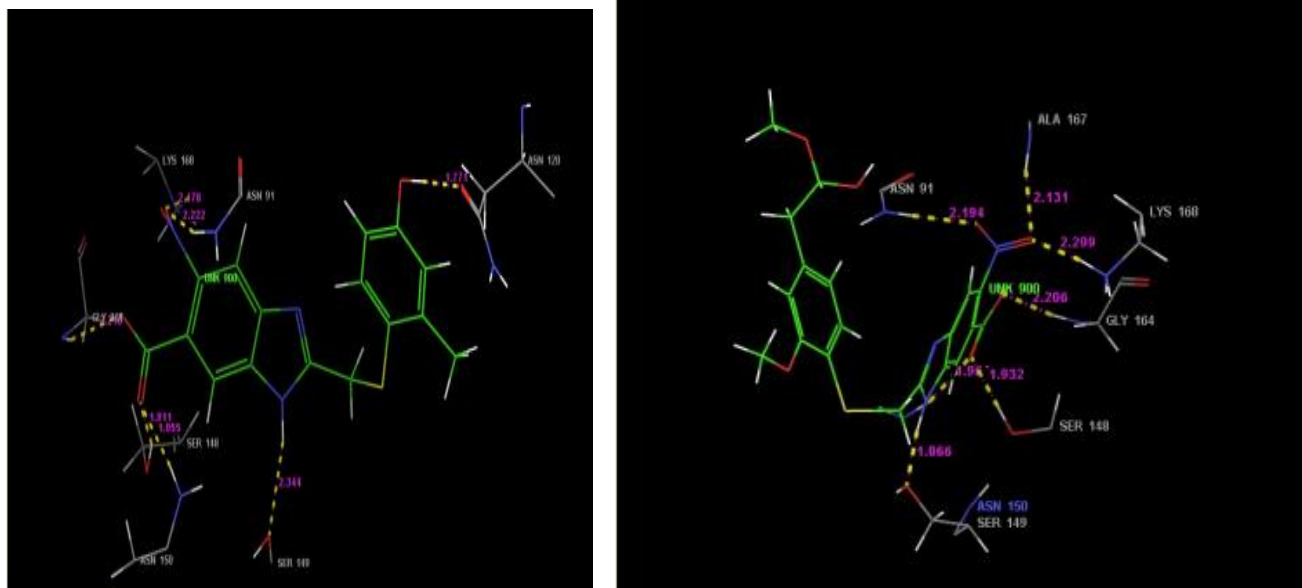


Fig. 7 Hydrogen bond interactions of molecule No. 25(left) and 28(right) with TOPO2 at ATPase binding site. Molecule 28 shows 7 hydrogen bond while Molecule 25 also shows 7 hydrogen bond.

281

Compared to the conventional co-crystallize ligand ANP in the PDB reported in Table 8, more than 5 compounds exhibit higher G scores. Comparing these 5 compounds to the normal ANP and Novobiosine presented in Fig. 8 as follows, they exhibit similar amino acid interactions, such as Asn91, Asn120, Lys 168, Gly 164, Ser 148, Ser 149, and Asn150.

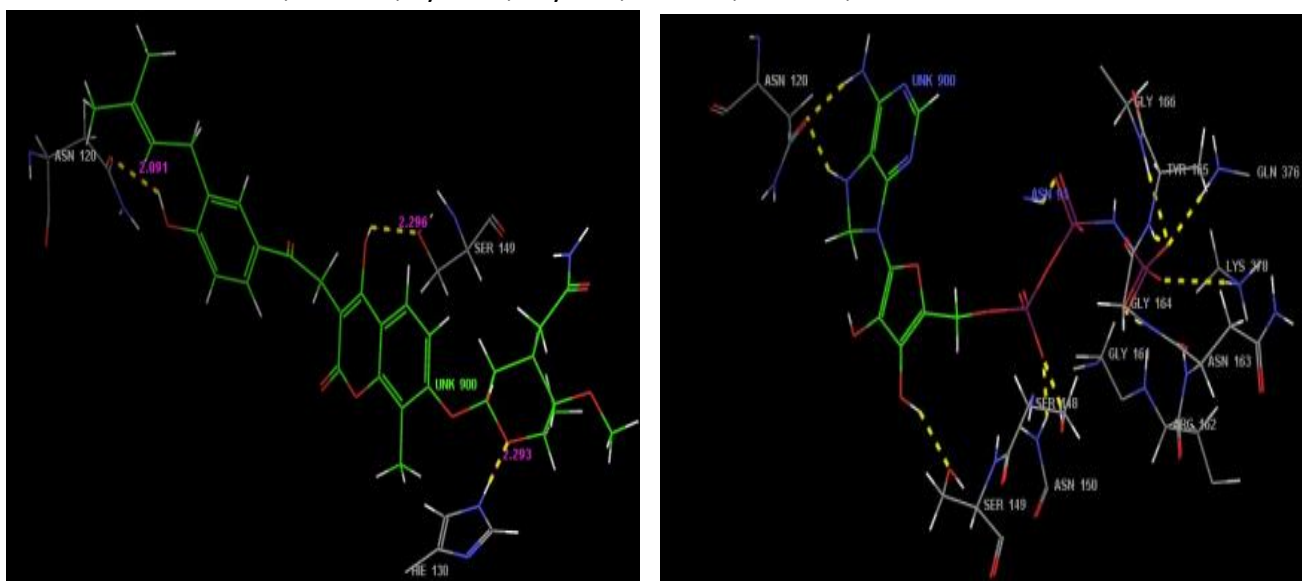
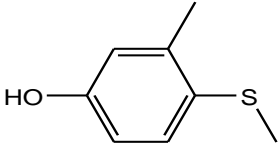
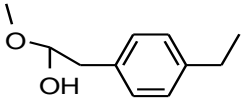
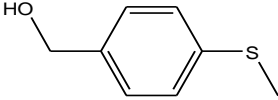
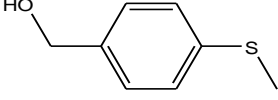
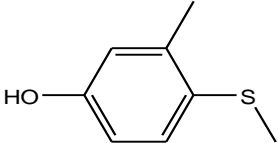


Fig. 8 Hydrogen bond interactions of (a)Novobiosine (b) ANP

Table 8 : Key interactions between NCEs and Topo2 ATP binding pocket.

Sr.	Molecule	R ₄	R ₃	R ₂	H-bond interaction with distance in A°		Bonding group		G-score
							Functional Group	Amino acid Residue	
1	28	-NO ₂	-COOH		Asn9 1 Ala1 67 Lys1 68 Gly1 66 Ser1 48 Ser1 49	2.19 2.13 2.29 9 2.20 6 1.93 2 1.86 6	NO ₂ NO ₂ NO ₂ COOH COOH HN	HN HN HN HN HO HO	-10.02
2	25	-NO ₂	-COOH		Asn9 1 Asn1 20 Lys1 68 Gly1 64 Ser1 48 Ser1 49 Asn1 50	2.22 2 2.17 8 2.47 82 2.21 6 1.91 1 2.34 4 1.95 5	-NO ₂ OH NO ₂ COOH COOH HN COOH	HN C=O HN HN HO HO HN	-9.93



3	80	- COOH	-NO ₂		Ala1 67 Asn1 20 Gly1 64 Gly1 66 Ser1 48 Ser1 49 Asn1 50	2.04 3 1.73 8 2.17 2.11 5 2.01 6 2.33 4 1.97 8	COOH CH ₂ OH COOH COOH -NO ₂ HN -NO ₂	HN C=O HN HN HO C=O HN	-9.90
4	56	Hydro xy	-NO ₂		Asn1 20 Ser1 48 Ser1 49 Asn1 50	1.81 2 1.50 4 2.41 5 1.79 1	CH ₂ OH HO HN C=O	C=O HO C=O HN	-9.87
5	55	Hydro xy	-NO ₂		Asn9 1 Gly1 64 Asn1 50 Ser1 49Se r148 Asn1 20	2.29 2.48 1.76 5 2.09 1.73 1.53 2	-NO ₂ -NO ₂ HO HN OH OH	HN HN HN C=O HO C=O	-9.83
Stan dard	ANP	--	--	--	Asn1 20 Asn1	2.01 1.92 1.95	HN HN HO	C=O C=O HO	-9.82



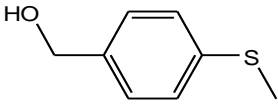
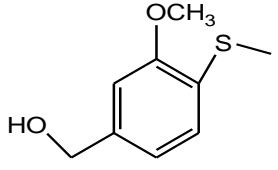
8	26	-NO ₂	-COOH		Ser1 49 Ser1 48 Asn1 20 Gly1 64 Gly1 66 Asn1 50 Lys1 68	2.32 1.91 1.89 2 2.20 1 2.19 1.94 1 1.99	-NO ₂ -NO ₂ -OH -NO ₂ -COO -NO ₂ -COO	-OH -OH C=O -NH -NH -NH -NH	-9.70
9	82	- COOH I	-NO ₂		Gly1 13 Gly1 12 Val1 17 Lys1 09 Asn4 5	1.8 2.46 1 2.46 2 2.41 2 1.92	C=O C=O -NH S -OH	-NH -NH C=O -NH C=O	-9.67
Stan dard	Novob iosine	--	--	--	Hie1 30 Ser1 49 Asn1 20	2.29 3 2.29 6 2.09 1	Morpholin e-O -OH -OH	-NH -OH C=O	-8.55

Table 7 lists the developed compounds' G scores, which were higher than the G-scores of the benchmarks ANP and Novobiocine (G score: -9.82, and -8.55 respectively). The

poses of ligand-receptor interactions discovered in docking investigations of NCEs and conventional medications are reported in Figures 7 and 8. In the ANP binding



pocket, all designed compounds adopted similar conformations to those of standard compounds. Docking studies revealed that all ligands are located in the same hydrophobic pocket of the Topoisomerase II enzyme's ATPase binding site, which contains the amino acids Asn91, Asn120, Lys 168, Gly 164, Ser148, Ser149, and Asn150. Thusly created compounds displayed good binding affinity for interacting with Topoisomerase II enzyme's ATPase binding site.

To punish the G-score and overall ligand conformation while binding to active binding amino acid residues in all the unfavourable and ugly interactions. Additionally, the model's energy is penalised by this. And because G-score is calculated by taking into account all of the aforementioned factors, we took every precaution when designing new chemical entities to inhibit Topoisomerase II's ATP hydrolysis more effectively and, as a result, to optimise the pharmacophore needed to significantly inhibited the enzyme's catalytic activity.

Both physicochemically significant descriptors and pharmacokinetically

important features can be predicted using the QikProp programme. Additionally, it assesses the acceptability of analogues in accordance with Lipinski's Rule 5 (40, 41), which is crucial to guaranteeing a medication's similar pharmacokinetic profile when utilising rational drug design. According to Lipinski's Rule 5, every structure displayed significant values for the examined attributes and displayed drug-like characteristics. The ADMET values of design compound inhibitors are shown in Table 9.

The first three characteristics—molecular weight (mol MW) less than 650, octanol and water partition coefficient (logPo/w) between -2 and 6.5, and solubility (qplogS) greater than -7—are based on the Lipinski rule of five. The brain/blood partition coefficient (QPlogBB) measure, which is required apparent MDCK cell permeability in nm/sec, provided information on the drug's capacity to cross the blood brain barrier. The blood-brain barrier is thought to be well mimicked by MDCK cells. Increased cell permeability All of the proposed compounds displayed acceptable ADME properties.

Table 9:- Table showing details of ADME prediction of top 15 designed compounds of benzazole series and with standard.

Comp.no	Mol.MW	Log P0/w	Log S	Log BB	PMDCK	% Absorbtion	Oral	Rule of five
028	433.43	2.79	-4.82	-2.97	494.2	92.13		0
080	359.35	1.84	-4.21	-2.65	363.8	68.945		0
056	331	1.7	-4.06	-2.182	263.49	79.34		0
055	351.33	1.97	-4.305	-2.128	228.65	80.34		0



079	359.45	2.07	-4.43	-2.58	413.07	99.965	0
026	359.31	1.83	- 4.177	-2.64	433.06	89.63	0
082	434	1.18	- 4.828	-2.97	354.22	93.75	0
058	405.42	2.159	-4.78	-2.47	640.26	92.52	0
047	373.38	2.15	- 5.416	-1.606	1938.312	86.96	0
002	344	3.54	- 4.364	-1.836	253.748	73.102	0
083	369	2.27	- 4.004	-2.004	182.862	86.83	0
029	359.83	2.815	- 4.683	-1.99	162.89	96.33	0
004	418.4	2.885	- 5.017	-2.1	127.675	72.6	0
060	289.3	2.2	-3.92	-1.4	124.613	80.75	0
025	359.13	2.07	-4.43	-2.58	153.08	78.63	0
Novobiosine	595	1.43	- 4.963	-3.74	162.12	65.23	0

The best five compounds i.e 28, 25,80,55,56 that follow the all screening criteria were selected for further study and biological evaluation for cross verifying the result of Molecular modelling studies.

Experimental work.

Computational details:

V-Life Sciences MDS Version 2.0.30 was used for all computational analyses. The compounds were built using the V-life molecular Builder database's fragments, which had standard bond lengths and bond angles. Geometry optimization was done using the standard Merck Molecular Force Field (MMFF) 31, which had a distance dependent-dielectric function and an energy gradient of 0.001 kcal/mol. Using

the Powell technique, the initial conformations were chosen and reduced until root-mean-square The results showed a deviation of 0.001 kcal/mol. The Gasteiger formula was used to determine partial atomic charges. Each compound underwent additional geometry optimization using the MOPAC 6 programme and the semi-empirical AM1 Hamiltonian. 32

2D-QSAR studies

Invariable columns were eliminated, and several descriptors were generated. Partial least squares (PLS), Principle component regression (PCR), and multiple linear regression (MLR), along with simulated annealing (SA), were used to carry out the 2D-QSAR. Using SA-PLS, SA-PCR, and SA-



MLR combinations, several 2D QSAR models were created 32, 33. Compared to SA-PLS and SA-PCR, the SA-MLR produced the superior modelling and prediction efficiency **3D-QSAR kNN MFA.**

Alignment

Using a template-based strategy, alignment was carried out³⁴. Compound alignment is a crucial component of the 3D QSAR approach and, consequently, of the kNN MFA analysis. At each lattice intersection of a uniformly spaced grid box, the steric and electrostatic potential fields for kNN-MFA³⁵ were determined for each alignment. A value of 2.0 was chosen for the lattice spacing in the X, Y, and Z directions. The dielectric constant, which varies with distance, was set at 1.0. In order to calculate the steric and electrostatic forces, an sp³ carbon atom with a Van der Waals radius of 1.52 and + 1.0 charge was used as the probe atom.

Generation of 3D- QSAR models-

The optimal number of components was determined using the standard kNN approach in combination with the cross-validation (leave-one-out) ^{36,37}option, which was then applied to derive the final 3D-QSAR model with cross-validation. The kNN MFA approach was used to create the 3-D QSAR models.

About k Nearest Neighbor Molecular Field Analysis (kNN-MFA)-

An unknown member is classified using the majority of its k-nearest neighbours in the training set according to the kNN methodology, which relies on a straightforward distance learning approach.

The proximity is quantified using the proper distance metric (e.g., a molecular similarity measure calculated using field interactions of molecular structures). Implementing the standard kNN approach is as easy as the following. (26)

(1) Determine the separations between an unknown item (u) and each of the training set's objects.

(2) Based on the estimated distances, choose k objects from the training set that are most similar to object u. (3) Classify object u with the group to which the majority of the k objects belong.

A test set of samples' classification or leave-one-out (LOO) cross-validation is used to identify an appropriate k value. Various variable selection techniques, as discussed below, were used to pick the variables and ideal k values.

Simulated annealing with kNN-MFA: Simulated annealing (SA) simulates the actual process known as "annealing," which includes heating a system to a high temperature and then gradually lowering it to a predetermined temperature (e.g., room temperature). In order to achieve equilibrium with the highest density of low energy states, the system samples several configurations distributed according to the Boltzmann distribution during this process.

The SA kNN-MFA approach combines the SA variable selection process with the kNN classification principle. Using stochastic sampling and simulated annealing as an optimization tool, it aims to optimise the following for each predefined number of variables (V_n):



- (i) The number of nearest neighbours (k) used to estimate each molecule's activity and
- (ii) The choice of variables from the initial pool of all molecular descriptors that are used to calculate similarities between molecules (i.e., distances in Vn-dimensional descriptor space).

Design of new chemical entities using Leadgrow tool

The Benzazole nucleus was optimised for selective inhibition of the TOPO2 inhibitors using the knowledge gained from 2D and 3D QSAR experiments. To ensure that the planned NCEs had a pharmacokinetic profile similar to that of a medication, the following filters were applied when creating CombiLib.

A = Number of hydrogen Bond Acceptor (Not more than 8)

D = Number of Hydrogen Bond Donor are in range (Not more than 5)

R = Number of Rotatable Bond are in range (Not more than 10)

X = XlogP is in ideal range < 5

W = Molecular Weight is in ideal range < 500 Da

S = Polar surface area), (Not more than 60 Å²)

Polar surface area that is dynamic (PSAd) (S), (not more than 60 2) The CombiLib tool of MDS generated more than 500 compounds using the Lipinski's rule-compliant templet (Fig. no. 6). The word ADRXWS in Table 7's columns holding the Lipinski score (1-6) and the other column

containing the strings of alphabets ADRXWS show that the relevant compound qualifies all of the required parameters established for Lipinski's screen filter. If molecules do not meet all six requirements, the corresponding numbers of alphabet strings are removed from the column and the screen score is lowered, indicating a lower degree of pharmacokinetic compatibility for that substance.

Docking studies-

Glide (5.0)³⁹ molecular docking programme was used for the molecular docking research. According to an earlier approach described by one of the coauthors, the most active compounds were chosen and docked onto the crystal structure of human topoisomerase II (RCSB PDB Database, Code: 1ZXM), which was cocrystallized with the ligand adenosine nucleotide triphosphate (ANP). In order to ascertain whether NCEs and the enzyme on PDB could interact, molecular docking studies are used (1ZXM).

ADME Prediction

One of the most crucial steps in the development of the therapeutic molecule is the prediction of the ADME parameter before the experimental research. If the drug candidate does not possess such qualities, the medicine may not advance to the market phase. Using the QikProp43 3.0 software, the ADME profile of the developed NCEs was examined while taking into account the aforementioned factor.

The absorption, distribution, metabolism, and excretion (ADME) prediction tool QikProp in Maestro and Schrodinger was



utilised in this case to forecast the ADME parameters. Using either individual or batch analysis, QikProp forecasts the physically significant descriptors and pharmaceutically significant features of organic compounds. besides predicting molecular characteristics. For comparing a specific property with that of 95% of known medications, QikProp offers ranges. QikProp was used to examine 40 physically important features of benzazole analogues, of which major descriptors were published here and are necessary for predicting the drug-like properties of compounds. These properties were

- 1.Molecular Weight (mol_MW) (150-650)
- 2.Octanol/Water partition coefficient(Log P_{o/w}) (-3.0-1.2)
- 3.Aqueous solubility (QPlog S)(-6.5-0.5)
- 4.Apparent MDCK cell permeability (QPPMDCK) (<25poor,>500great)
- 5.Brain/blood partition coefficient (QPlogBB)(-3.0-1.2)
- 6.Percent Human Oral absorption (>80% is high,<25%is poor).

Conclusion:-

We were able to determine the electronic, steric, hydrophobic, and topological characteristics of the substitution pattern surrounding the chosen benzazole pharmacophore through careful examination of the findings of 2D and 3D QSAR investigations. With the aid of a 2D QSAR regression equation and the information provided, New Chemical Entities (NCEs) were built using the

CombiLib tool, and the designed NCEs' activities were also calculated.

We had to set filters like molecular weight, logP, number of H-bond donors, number of H-bond acceptors, polar surface area, and number of rotatable bonds to ensure that only drug like NCEs would be generated and that the resulting NCEs would not have the pharmacokinetic deficiencies. This was because drug like pharmacokinetic profile set up was the main cause of NCE failure at later stages of the drug discovery process. In order to assess the NCEs produced by combiLib, Lipinski's screen was used. According to the results, designed NCEs meet every requirement for Lipinski's screen. To get more understanding of how NCEs interact with the ATPase binding pocket on topo II, the most powerful derivatives were put through molecular docking studies.

Both physicochemically significant descriptors and pharmacokinetically relevant features are predicted using the QikProp tool. Additionally, it assesses analog's acceptability using Lipinski's Rule 540,41. It is necessary to guarantee that a medicine has a certain pharmacokinetic profile when utilising a rational drug design. In the current study, we use molecular modelling to show that benzazole compounds block human topo II catalytically by attaching to the ATP domain. This prevents DNA cleavage and inhibits ATP hydrolysis. To determine the validity of the reasoning behind the creation of NCEs in general and the optimization of the pharmacophore for the



selective catalytic inhibition of topo II in particular, the results of dry lab work will be thoroughly reviewed.

Acknowledgement

The authors are extremely grateful to Professor Dr. Bhandari Sir for providing us with thorough insights into works using molecular modelling. The principal Dr. Sanjay Walode of our institute, RMDIPER, is also acknowledged by the authors for providing the required facilities and serving as a constant source of inspiration and encouragement.

Supporting Data

Supporting information NCEs produced by the Lead Grow tool and the findings of the molecular docking analyses of the generated NCEs are included in Tables 1 and 2, respectively,

References:-

- 1.Brill, S. J., Dinardo, S., Voelkel-Meimanam, K. and Sternglanz, R., Nature, 1987, 326, 414–416.
2. Newport, J., Cell, 1987, 48, 219–230.
3. Wang, J. C. and Lynch, A. S., Curr. Opin. Genet. Dev., 1993, 3, 764–768.
4. Wang, J. C., Annu. Rev. Biochem., 1985, 54, 665–697.
5. Watt, M. P. and Hickson, D. I., Biochem. J., 1994, 303, 681–695
6. D. Jayaraju and Anand K. Kondapi CURRENT SCIENCE, VOL. 81, NO. 7, 10 OCTOBER 2001 pg no.787 -792
7. G. Capranico, F. Zunino, DNA topoisomerase-trapping antitumour drugs, Eur. J. Cancer 12 (1992) 2055^2060.

8 .A.H. Corbett, N. Osheroj, When good enzymes go bad: conversion of topoisomerase II

to a cellular toxin by antineoplastic drugs, Chem. Res. Toxicol. 6 (1993) 585-597.

9.A.Y. Chen, L.F. Liu, DNA topoisomerases: essential enzymes and lethal targets, Annu. Rev. Pharmacol. Toxicol. 34 (1994) 191-218.

10. L. Liu, DNA Topoisomerases: Topoisomerase-Targeted Drugs, Vol. 29, Academic Press, New York, 1994.

11.S.J. Froelich-Ammon, N. Osheroj, Topoisomerase poisons: harnessing the dark side of enzyme mechanism, J. Biol. Chem. 270 (1995) 21429^21432.

12 .B.K. Sinha, Topoisomerase inhibitors: a review of their therapeutic potential in cancer, Drugs 49 (1995) 11-19.

13. H. Malonne, G. Atassi, DNA topoisomerase targeting drugs: mechanisms of action and perspectives, Anti-Cancer Drugs 8 (1997) 811^822.

14. Y. Pommier, in: B.A. Teicher (Ed.), Cancer Therapeutics: Experimental and Clinical Agents, Vol. I, Humana Press, Totowa, NJ, 1997, pp. 153-174.

15.Annette K. Larsena,, Alexandre E. Escargueil, Andrzej Skladanowski, Catalytic topoisomerase II inhibitors in cancer therapy, Pharmacology & Therapeutics 99 (2003) 167– 181

16.K.G. Miller, L.F. Liu, P.T. Englund, A homogeneous type II DNA topoisomerase from HeLa cell nuclei, J. Biol. Chem. 176 (1981) 9334-9339.

17.K. Shiozaki, M. Yanagida, A functional 125-kDa core polypeptide of ψ ssion yeast



DNA topoisomerase II, *Mol. Cell. Biol.* 11 (1991) 6093-6102

18.K. Shiozaki, M. Yanagida, A functional 125-kDa core polypeptide of *S. cerevisiae* DNA topoisomerase II, *Mol. Cell. Biol.* 11 (1991) 6093-6102.

19.J.M. Berger, Type II DNA topoisomerases, *Curr. Opin. Struct. Biol.* 8 (1998) 2632.

20.kinase II phosphorylates the eukaryote-specific C-terminal domain of topoisomerase II in vivo, *EMBO J.* 11 (1992)1785-1796.

21. M.M. Heck, W.N. Hittelman, W.C. Earnshaw, Differential expression of DNA topoisomerases I and II during the eukaryotic cell cycle, *Proc. Natl. Acad. Sci. USA* 85 (1988) 1086-1090.

22. Sandhiya Patel, Elen Jazrawi, Andrew M. Creighton, Caroline A. Austin, And L. Mark Fisher. Probing the Interaction of the Cytotoxic Bisdioxopiperazine ICRF-193 with the Closed Enzyme Clamp of Human Topoisomerase IIa *Molecular Pharmacology* Vol. 58, No. 3 82848105

23. John L. Nitiss, Targeting DNA topoisomerase II in cancer chemotherapy, John L. Nitiss

24.Pommier Y, Kerrigan D, Schwartz RE, Swack JA, McCurdy A. Altered DNA topoisomerase II activity in Chinese hamster cells resistant to topoisomerase II inhibitors. *Cancer Res* 1986;46:3075–81.

25. Danks MK, Schmidt CA, Cirtain MC, Suttle DP, Beck WT. Altered catalytic activity of and DNA cleavage by DNA topoisomerase II from human leukemic cells selected for resistance to VM-26. *Biochemistry* 1988;27:8861–8879.

26. Lage H, Helmbach H, Dietel M, Schadendorf D. Modulation of DNA topoisomerase II activity and expression in melanoma cells with acquired drug resistance. *Br J Cancer* 2000;82:488–91.

27. Jds M, Deisseroth K, Mayes J, Altschuler E, Jansen R, Ledley FD, welling LA. Identification of a point mutation in the topoisomerase II gene from a human leukemia cell line containing an amsacrine-resistant form of topoisomerase II. *Cancer Res* 1991;51:4729–31.

28.Ermann Lage¹, Esin Aki-Sener² and Ismail Yalcin² High antineoplastic activity of new heterocyclic compounds in cancer cells with resistance against classical DNA topoisomerase II-targeting drugs, *Int. J. Cancer*: 119, 213–220 (2006).

29.lem Temiz-Arpaci, Betul Tekiner-Gulbas, Ilkay Yildiz,* Esin Aki-Sener and Ismail Yalcin, 3D-QSAR analysis on benzazole derivatives as eukaryotic topoisomerase II inhibitors by using comparative molecular field analysis method, *Bioorganic & Medicinal Chemistry* 13 (2005) 6354–6359.

30. VLifeMDS, Molecular Design Suit Version 2.0, V-Life Science Technologies Pvt.LTD. Pune, India, 2004,(www.vlifesciences.com).

31. T. A. Halgren, , *J. Comp. Chem.* 1996, 17, 520–552.

32. K.Ohtawara and H.Teramae, *Chemical physics Letters*, 2004, 390, 84-88

33. S.Bhandari, K. Bothara, S. Gore, C. Khachane, A. Sarkate, A. Patil, *Proceedings of the European Symposium on Quantitative Structure-Activity Relationships &*



Omics Technologies and Systems
Biology, Uppsala, Sweden, Sept. (2008)

34. S.Vengurlekar, R.Sharma and P.Trivedi
Medicinal Chemistry
Research, 2009, DOI:10.1007/s00044-009-
9256-y

35. S. Ajmani, K. Jadhav, and S. Kulkarni: J.
Comp. Inf. & Model, 2006, 46, 24–31.

36. P.S.Charifson in Practical Application of
Computer-aided drug design, MARCEL
DEKKER INC, 1997, 112-113.

37. V. Vanheusden, H. Munier-Lehmann, M.
Froeyen, L. Dugue, A. Heyerick, d. Keukelcire
and S.Pochet, J. Med. Chem., 2003, 46,
3811-3821

38. Ajmani, K. Jadhav, S. Kulkari, J. Chem.
Inf. Comput. Sci. 40 (2006) 24-31.

39. Glide, Molecular Docking Tool of
Schrodinger Inc., Version 5.0, New York,
USA.

40. Fatma M. Abdel Bar, Mohamad
A. Khanfar,
Ahmed Y. Elnagar, J. Nat. Prod. 2009, 72, 1643-
1650.

41. Kontoyianmi, M.; McClellan, L.; Sokol, G. S. E
valuation of docking performance:
comparative data on docking algorithm.
J. med. Chem. 2004, 47, 558-565

42. Glide Molecular docking tool of
Schrodinger Inc., version 5.0, New York, USA

43. QikProp, Version 3.1, Schrodinger LLC,
New York.

